

A Methodology for Large-Scale Parametric Evaluation of Child Booster Seats

Matthew Miller, Daniel Perez-Rapela, Bronislaw Gepner, Marcy Edwards,
Jessica Jermakian, Jason Forman

Abstract Child booster seats vary in size, shape and material, and the effects of these parameters on occupant response are not well understood. Large-scale computational studies are a means to explore the effects of these parameters across the space of potential booster designs. This work lays the foundation for such large-scale studies by quantifying the current booster design space, implementing a booster parameterization methodology, and comparing results of simplified, parametric booster models with similar, existing finite element models. These parameterized boosters are integrated into a simulation pipeline that positions and settles a child human body model, routes the seatbelt, and runs a frontal impact pulse – all automated to allow user-free execution of hundreds of simulations spanning the booster design space. Results include measurements of a 44 booster test sample, which was constructed from a set of 20 booster seat parameters across the categories of booster geometry, construction, lap belt routing, shoulder belt routing, and subject posture. Simplified booster seats generated with the parameterization methodology demonstrated similar occupant response when compared to more complex finite element booster models. The automation pipeline proved to be a robust tool, allowing much larger studies to be undertaken than would be possible with a manual approach.

Keywords Booster, CRS, HBM, PIPER, Restraint.

I. INTRODUCTION

Motor vehicle crashes (MVCs) are a leading cause of death for children in the USA [1]. Children pose a restraint challenge, driven in part by the geometry of their belt fit and interaction with restraint systems as they grow throughout childhood. Belt-positioning booster seats aid in the transition as a child outgrows a dedicated child seat (with a multi-point harness) but is not yet tall enough to engage properly with a vehicle seat and seatbelt. Booster seats raise the child above the seat cushion and often reroute the lap belt, with the goal of improving occupant restraint engagement. Depending on their geometry, they may also assist in placing the shoulder belt in the desired location on the shoulder, instead of higher on the neck. The American Academy of Pediatrics recommends that children use belt-positioning booster seats until they can properly engage with the vehicle seatbelt, which usually occurs around 8 years of age or older [2]. Booster seats have been shown to reduce risk of serious injury by 45% for 4–8-year-olds [3].

There is a large variability of designs in the booster seat space (Fig. 1). A child safety seat that is designed to function as both a forward-facing harness-equipped restraint and as a booster seat may look very different from a belt-positioning device that prioritizes transportability. As such, the design space for boosters and belt-positioning devices is quite broad, with little information available to understand the influence of various design characteristics on real occupant response.



Fig. 1. Various booster seat designs.

While they are valuable tools for physical testing, the current generation of paediatric anthropometric test devices (ATDs) have limited biofidelity in the pelvis and abdominal regions, particularly with regard to submarining [4-5]. This is a concern, as abdominal injuries are the second most common injury in young children in MVCs [6], and belt-induced injuries from “seatbelt syndrome” [7-8] and submarining [9-10] are well documented.

M. Miller (e-mail: mfm9wy@virginia.edu; tel: 1.434.297.8016) is a MSc student in Mechanical Engineering, D. Perez-Rapela is a Post-Doctoral Researcher, B. Gepner is a Research Scientist, and J. Forman is a Principal Scientist, all at University of Virginia, USA. M. Edwards is a Research Engineer and J. Jermakian is the Vice President of Vehicle Research at the Insurance Institute for Highway Safety, USA.

With the limitations of physical tools for booster seat testing, finite element (FE) simulations present a complementary avenue to evaluate how booster seat characteristics affect occupant response in an MVC. FE human body models (HBMs) have the potential for improved biofidelity without the constraints imposed by physical tools [11-12]. Recent FE studies relating to booster seats are generally limited to small sample sizes [13–15]. However, given the breadth of the booster design space, a very large number of simulations may be needed to capture potential non-linearities and interactions among the effects of various booster design characteristics. Such a large-scale, parametric study cannot be performed using traditional means, manually setting up and executing models. Instead, investigating such a broad parameter space requires development of an automated simulation pipeline capable of performing hundreds or thousands of simulations [12] to study occupant responses across the breadth of the potential booster design space. Information gained from these large-scale studies can be used to generate metamodels that capture the relationship between booster design parameters and occupant responses, gaining insight into the entire design space rather than just the individually simulated data points.

This work seeks to lay the foundation for future large-scale, parametric, FE booster seat simulation studies. Specifically, this study developed an automated simulation pipeline (free from human interaction) to generate a parametrically defined booster model, position a HBM occupant, route the seatbelt, and execute a collision simulation. Through this fully automated process, this method may be used to quantify the effects of key booster design characteristics on occupant responses across the potential design space, and to streamline the investigation of specific types of design.

II. METHODS

Automation Pipeline

A simplified booster generation process was implemented into the seven-step automation pipeline shown in Fig. 2. This automation expands on previously published work [12], with the parametric booster generation HBM positioning and seatbelt routing representing the largest differences. The automation pipeline was coded in MATLAB R2020a, leveraging resources from LS-DYNA v9.1.0 and LS-PrePost v4.6.21 where needed.



Fig. 2. Automation pipeline.

Booster Seat Data Collection

First, this study sought to collect geometric data on existing booster seats to inform the development of the parametric booster simulation tool. The term “booster” is used broadly here to include traditional booster seats and less traditional belt-positioning devices. Forty-four booster seats were evaluated, spanning the range of booster seats available in the US market. Categorical data were collected for each booster seat, including booster type, construction, type of lap belt guide, and type of shoulder belt guide. Appendix A details the booster models tested. Each booster was placed onto a rear-seat buck constructed from a 2004 Ford Taurus [16]. Three-dimensional coordinates of landmarks were collected with a coordinate measuring machine, and multi-point surface sweeps were collected for critical surfaces. In all, 20 different measurements were collected (Fig. 3).



Fig. 3. Booster measurement points and sweeps.

The three-dimensional coordinates of landmarks shown in Fig. 3 were imported into MATLAB for post-processing. A simplified profile contour of each booster was defined by manually identifying four points from the seatpan and seatback sweeps of each booster plot (Table I, Fig. 4). Two booster-specific coordinate systems were defined. The booster seatpan coordinate system was defined with the x-axis extending from the bight along the first segment of the booster seatpan, while the seatback coordinate system was defined with the x-axis extending from the bight along the seatback (Fig. 4). These coordinate systems were introduced so that the lap belt guide location could be measured relative to the first cushion segment, while the shoulder belt guide location could be measured relative to the booster seatback.

TABLE I
BOOSTER PROFILE POINT SELECTION

Point	Name	Description
1	Seatback	Point in line with portion of seatback that will interact with occupant’s shoulder
2	Bight	Intersection point between line along primary seatback section and seatpan
3	Seatpan Inflection	Point where slope of seatpan changes
4	Seatpan End	Point where seatpan turns downward

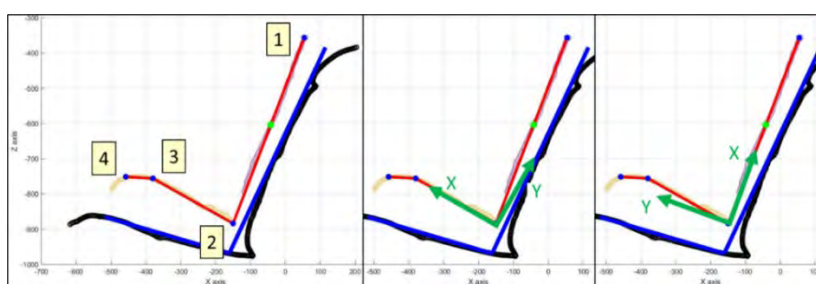


Fig. 4. Booster profile definition (left), seatpan CS (middle), seatback CS (right). Booster profile in red, bench profile in blue, coordinate systems in green.

Three types of shoulder belt guide were identified in the test sample: fixed shoulder belt guide, flexible shoulder belt guide, and free (Fig. 5). Four types of lap belt guide were identified in the test sample: wide lap belt guide, narrow lap belt guide, flexible lap belt guide, and fixed lap belt guide (Fig. 6). The flexible and fixed lap belt guide types are closed structures sized such that the belt cannot translate within the guide, and are differentiated by how they attach to the booster seat. The wide lap belt guide is an open structure with a wide opening allowing the belt freedom of movement within the structure. The narrow lap belt guide has a narrower overall structure and opening. Principal component analyses (PCAs) [17] were completed for all wide and narrow lap belt guide sweeps, producing a primary axis angle, primary axis length, and secondary axis length for each lap belt guide sweep. A representative lap belt guide was chosen for both the wide and narrow types by averaging the results of the PCA and picking the specific guide geometry that was closest to that average. The representative wide profile was from the Cybex Solution M-Fix Booster, while the narrow profile was from the Graco Argos80 booster.



Fig. 5. Types of shoulder belt guide: fixed shoulder belt guide, flexible shoulder belt guide, free (left to right).



Fig. 6. Types of lap belt guide: wide lap belt guide, narrow, fixed lap belt guide, flexible lap belt guide (left to right).

Angles and positions for the wide and narrow lap belt guides were determined by manually aligning the representative profile plot over the plot of each booster’s lap belt guide. Once in position, a MATLAB script was utilized to extract the centroid and angle of the corresponding final representative lap belt guide.

The collected data were used to generate a set of parameters capable of describing the booster design space. These parameters were separated into the following four categories: booster geometry, construction, lap belt routing and shoulder belt routing. Fig. 7 details the measurements for eight of the booster geometry parameters. Seatback depth at 300 mm above the booster bight was selected as the parameter to determine seatback angle as that is the approximate location that the HBM’s shoulders contact the seatback. Not shown in the figure is the cushion breadth measurement, which is defined as the distance between the lap belt guides.

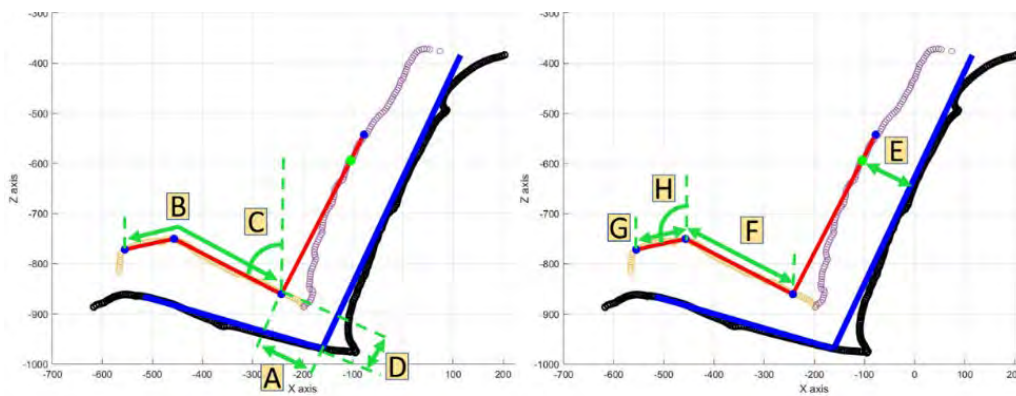


Fig. 7. Booster geometry parameters. (A) seatback depth at bight, (B) total cushion length, (C) cushion angle 1, (D) cushion depth at bight, (E) seatback depth at 300 mm, (F) cushion length 1, (G) cushion length 2, (H) cushion angle 2. Booster profile in red, bench profile in blue, measurement details in green.

Booster Seat Geometry Parameters and Sampling

Table II details the set of 20 parameters capable of describing the booster seat design space. Booster designs were generated from this set of parameters using a simulated annealing sampling algorithm that sought to maximize the space between each data point [12][18]. The range of measurements or categorical types observed in the sample is included, with all lap belt guide measurements performed in the seatpan coordinate system and all shoulder belt guide measurements performed in the seatback coordinate system (Fig. 4). These alternative coordinate systems allowed the belt guides to be measured relative to a reference frame defined by the booster geometry. Many booster parameters showed correlations with each other, and Table II details which of these correlations were considered during the sampling process. Correlations ranged from trivial (a backless booster always has a seatback depth of zero), to more subtle observations (seatback depth at bight and seatback depth at 300 mm have a positive linear relationship). Dependent parameters were sampled from adjusted ranges defined by the relationship with their associated independent variables. These correlations were accounted for in the sampling process to avoid the creation of unrealistic booster seat designs, while still preserving variability in the correlations (Appendix B). Booster mass (Parameter 13) was not determined during the sampling process. Instead, booster mass was determined by applying a density of 2.34e-7 kg/mm³ to the FE booster model. This value was calculated using the bulk volume and mass of the test sample boosters.

TABLE II
BOOSTER PARAMETER LIST

Category	#	Parameter	Recorded Range	Sampling dependent on
Geometry	1	Booster Type	Full, backless	Independent
Geometry	2	Seatback Depth at Bight	26.4 – 197.0 mm	1
Geometry	3	Total Cushion Length	207.9 – 405.7 mm	Independent
Geometry	4	Cushion Angle 1	55.8 – 84.6 deg	Independent
Geometry	5	Cushion Depth at Bight	31.6 – 142.8 mm	2
Geometry	6	Cushion Breadth	293.2 – 447.9 mm	Independent
Geometry	7	Seatback Depth at 300mm	48.2 – 141.3 mm	1, 2
Geometry	8	Cushion Length 1	107.1 – 288.2 mm	3

Geometry	9	Cushion Length 2	34.3 – 210.0 mm	3
Geometry	10	Cushion Angle 2	54.7 – 105.2 deg	4
Construction	11	Cushion Stiffness	Low, high	Independent
Construction	12	ISOFIX	Not fixed, fixed	Independent
Construction	13	Mass	0.25 kg – 11.32 kg	Not sampled
Lap Belt Routing	14	Lap Belt Routing Type	Wide, narrow, fixed, flexible	Independent
Lap Belt Routing	15	Guide Angle	-8.7 – 100.6 deg	14
Lap Belt Routing	16	Anterior/Posterior Position	20.6 – 206.4 mm	14, 17
Lap Belt Routing	17	Superior/Inferior Position	-3.9 – 87.2 mm	14, 16
Shoulder Belt Routing	18	Shoulder Belt Routing Type	Fixed, flexible, free	1
Shoulder Belt Routing	19	Anterior/Posterior Position	-71.0 – 74.2 mm	18, 20
Shoulder Belt Routing	20	Lateral/Medial Position	100.7 – 264.0 mm	18, 19

Additional parameters regarding the restraint environment were sampled as well. The lap belt anchor locations were independently sampled as either the “forward” or “aft” anchor positions detailed in the IIHS Booster Seat Evaluation Protocol. These values are based on the ranges observed in recent model test vehicles [19]. The shoulder belt anchor location was set at the location defined by FMVSS 213, as the shoulder belt anchor location was not a parameter of primary interest in this study. Future work may add variability to the shoulder belt anchor location by using the anchor positions defined in the IIHS Booster Seat Evaluation protocol. Booster constraint was sampled as well – boosters were either sampled as unconstrained, or constrained via ISOFIX attachment.

HBM slouching posture was also varied. Slouching posture was defined based on the distance between the posterior superior iliac spine (PSIS) of the pelvis and the booster seatback in the case of a full booster, or between the PSIS and the bench seatback in the case of a backless booster. A baseline upright posture was defined as having a 19 mm gap between the pelvis and seatback [19]. The posture value was independently sampled as either an upright, moderate slouch (shift pelvis 25 mm forward), or extreme slouch posture (shift pelvis 50 mm forward) (Fig. 8). These values were selected to represent a range of postures observed in volunteer tests [20].



Fig. 8. HBM posture comparison. Upright posture, moderate slouch, and extreme slouch (left to right).

Simplified Booster Generation

An FE model of the updated FMVSS 213 bench was developed for use in this study (Appendix C). A MATLAB script was then written to automatically generate an FE booster model from the set of sampled parameters. The script interfaced with LS PrePost to implement the geometry, mesh, material and constraints of the booster.

The booster profile was determined using the sampled parameters from the booster geometry category. The width of the booster cushion was defined by the cushion breadth parameter, while the width of the seatback was determined by the distance between the shoulder belt guides. A covering of shell elements was applied to the upper and lower surfaces of the booster cushion, as well as the front and aft surfaces of the booster seatback. These surfaces were implemented to improve the contact definition between the booster and its surroundings, as well as to mimic booster construction observed in the test sample. This resulted in a total of six parts for full boosters, and three parts for backless boosters. A hexahedral mesh was created for each booster once the overall geometry was determined. This mesh had a target edge length of 10 mm for each element, with a minimum edge length of 4 mm and a minimum of three elements across the depth of the cushion and seatback. Finally, the connection between cushion and seatback was modeled as a revolute joint. This joint was locked by adding adjacent nodes on the cushion and seatback to a constrained nodal rigid body. The joint was modeled in this way so that it could be freed in future analyses to examine the effects of cushion/seatback joint stiffness. Two general types of material were observed in the booster seat test sample. Traditional boosters made of plastic were defined as “high stiffness” boosters, while inflatable and foam booster seats were defined as “low stiffness” boosters. Separate material models were developed for these two types.

The booster provided with the PIPER model was used as the reference for high stiffness boosters. PIPER's torso and thighs were rigidized and used as an indenter to measure the stiffness of the PIPER booster up to a displacement of 100 mm. A simplified booster was then generated with the same external dimensions of the PIPER booster, and indenter simulations were run to tune the material parameters of the simplified booster. A low-density foam (LDF) material model was selected for the low stiffness boosters. Though some of the boosters in the parameter identification study were inflatable, the low-density foam material model was more easily integrated into the automation process than an airbag material model. Similar to the process above, the material properties of the low-density foam were tuned to result in an overall stiffness similar to what would be expected from an inflatable booster. Simulations were conducted to tune the LDF to exhibit the same stiffness of a simplified airbag model. A cube of airbag material was given an internal pressure equal to the maximum expiratory pressure of an adult male [21]. The compressive stiffness of this cube was recorded up to a deformation of 55%. Simulations were then run on a cube of LDF material, allowing material parameters to be tuned until the stiffness responses matched. The overall response was then checked through matched simulations with LDF boosters and airbag boosters of similar geometries, verifying that the HBM responses were generally similar.

Results of the high stiffness and low stiffness material model tuning tests are shown Fig. 9. An elastic material model with a Young's Modulus of 2 MPa was selected for the high stiffness material model, as it showed similar stiffness up to a 40 mm indentation. Booster indentations of more than 40 mm are not expected when subjecting the boosters to an FMVSS 213 pulse. The low stiffness booster tuning process resulted in a low-density foam material with a Young's modulus of 44.16 MPa.

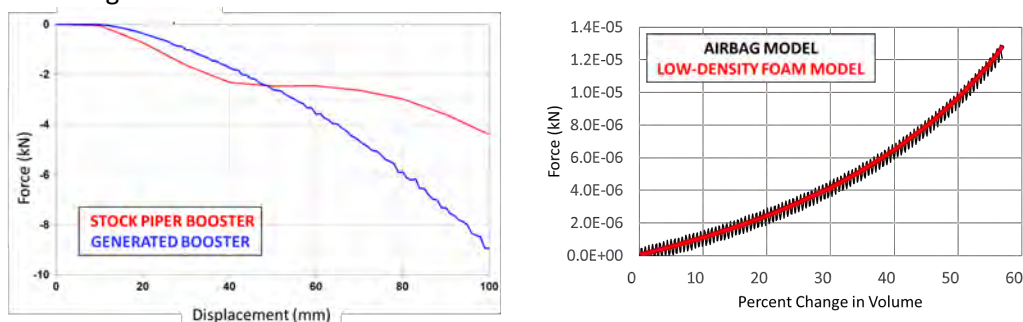


Fig. 9. Material tuning simulation results for high stiffness model (left) and low stiffness model (right).

In addition to the booster geometry, lap belt anchor geometry, booster material and occupant posture, the booster models were further parametrized based on constraint of the booster to the seat – either unconstrained or constrained via ISOFIX. The constrained case was modeled after ISOFIX rather than LATCH, as ISOFIX represents the extreme case of available booster constraint systems. For ISOFIXed boosters, the cushion was constrained to a rigid body fixture located posterior to the bench. This fixture was connected to the entire rigid bottom of the cushion for high stiffness boosters, or to a group of nodes at each end of the fixture in the case of low stiffness boosters. ISOFIXed boosters were free to rotate around the axis of the fixture, but were restricted from translation. Fig. 10 shows the constraints applied to the booster models.

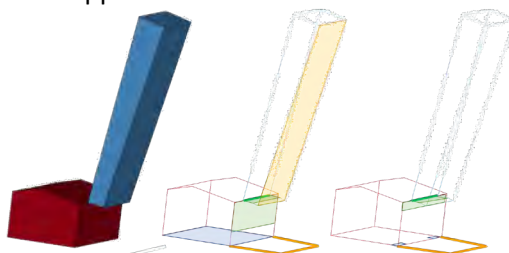


Fig. 10. Booster constraints for high stiffness boosters (center) and low stiffness boosters (right). Rigid bottom cushion (blue), ISOFIX (orange), seatback joint (green), rigid seatback (yellow).

HBM Positioning

The PIPER HBM [22] was selected for use in this study due to performance in validation cases relevant to frontal impacts, and its proven ability to submarine [23]. A MATLAB script was created to position the HBM relative to each booster model and bench. Proper positioning is critical to minimize the amount of simulation time required to settle the model. Nine initial simulations were run to prepare a seeding catalog of potential HBM pre-settling positions. These positions include five different recline angles and six different knee extension positions. In order to achieve these pre-settling positions, the models were initially rotated as a whole to achieve five different recline angles. The legs of each model were later rotated back to their original position by constraining the upper

body from T12 upwards and prescribing motion to the tibia, fibula and feet bones. Once the lower extremities were positioned, a second simulation was conducted on each of the five models to move the legs upwards to full extension by constraining the body from femur upwards (leaving the soft tissue of the lower extremities unconstrained) and prescribing motion to the distal tibia. The nodal positions were extracted at six different degrees of leg extension to define six models per recline angle. The pre-stress was not carried from one pre-positioning simulation to the other as this could make the model move back to its original upright position during the settling process. This process resulted in a total of thirty different seeds in the pre-settling model catalog (Fig. 11). The automated five-step process (Appendix D) then transformed, translated and rotated the model, as well as selected the closest initial position PIPER model from the 30 initial positions. This algorithm brought the models as close as possible to the final settled positions without interfering with the booster or bench (Fig. 12). The final output positions of the PIPER HBM were extracted for each booster and used as the initial positions for the settling simulations.

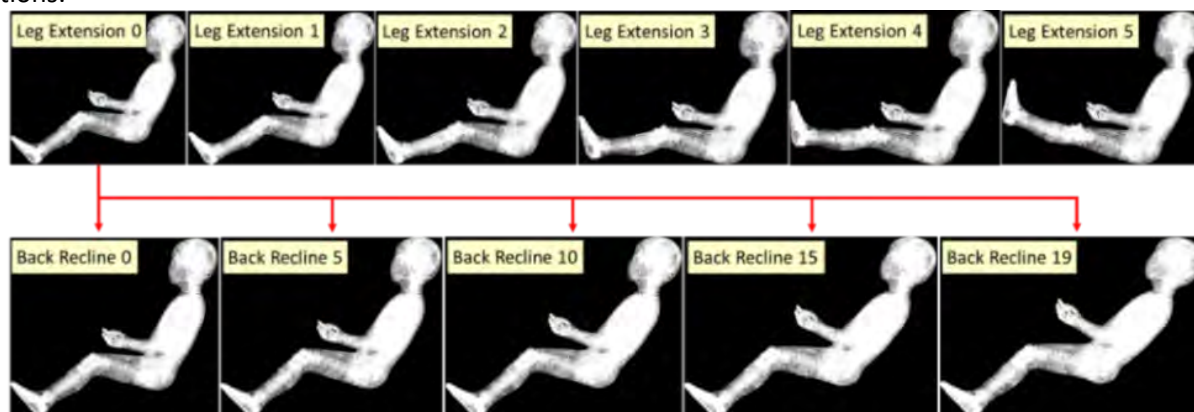


Fig. 11. HBM initial seed positions. Each leg extension seed also had five possible recline positions, totaling 30 seed positions. These are used to search for the closest initial position to reduce settling computation time.

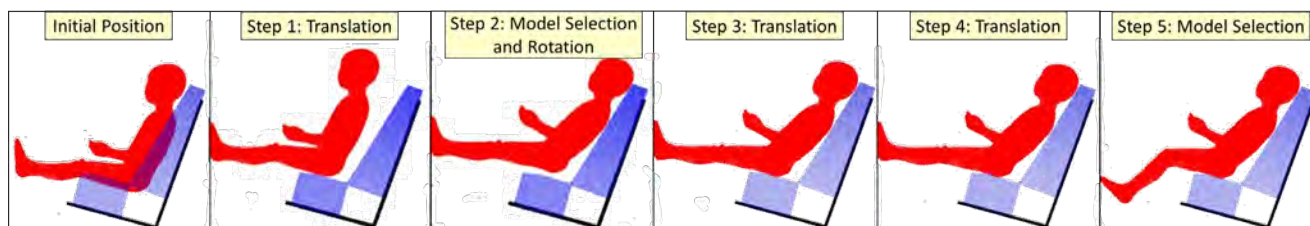


Fig. 12. HBM initial position searching example. HBM nodes in red, booster nodes in blue. Target position defined by a combination of the slouch target (distance between the pelvis and the seatback) and the recline and leg angles that result in the closest distance to the booster without penetration. This example did not require position adjustment in Step 4.

Settling Simulation

The purpose of settling simulations are to generate realistic equilibrium positions of the HBM, booster and bench prior to running the belt fitting and final simulations. The simulations are subjected to the force of gravity, allowing for interaction between parts as unconstrained bodies move downwards. Once the bodies reach equilibrium, the settled positions and stress states of each part are extracted. For this study, the final positions and stresses of the HBM, booster and bench were extracted and used as input conditions for the final simulation.

Each individual booster was located relative to the bench such that a 2 mm gap existed between the booster seat and the bench, perpendicular to the surface of the bench. The final seed posture determined by the algorithm in Fig. 12 was used as the initial HBM position for the settling. The HBM's pelvis was constrained such that it could rotate but could not translate away from the seatback, maintaining the HBM's target slouch posture distance throughout the settling. Additional HBM constraints used in the settling process are detailed in Appendix E. The PIPER model was given an initial velocity of 0.65 m/s downward along the seatback axis to speed the settling process, reducing the computational time of each settling simulation. Initial testing determined that this value was an appropriate balance between reducing the time requirements of the simulation without adding large amounts of additional energy to the simulation. Translational damping forces in the global z direction were applied to all nodes belonging to the PIPER model. This damping was implemented to discourage repeated oscillation of the model and to achieve equilibrium quickly. Initial testing indicated that a damping constant of 0.15 was a suitable value to approach a critically damped response across the range of input geometries and materials, and 400 ms was determined to be an appropriate settling simulation length using a test of 30 boosters.

Seatbelt Routing Simulation

The purpose of the seatbelt routing simulation was to generate realistic seatbelt positions relative to the HBM and booster, capturing the routing effects of the geometry of the booster, booster belt guides, belt anchor location, and HBM position. The final HBM position from the settling simulation was extracted and rigidized surfaces were defined for the torso, thighs and left arm. The torso and thigh surfaces were then pushed into a seatbelt that was being tightened, and the left arm was translated into its place sweeping in from the left. During the fitting simulation, the belt was also constrained by the appropriate slings and/or surfaces defined to represent the booster belt guide selected for that particular booster (sampled based on type and location). The simulation was complete when the PIPER model returned fully to its original position and the belt reached its final anchored positions. The final position of the seatbelt was then extracted, post-processed and added to the model prior to running the final simulation. Appendix F provides additional detail regarding this process.

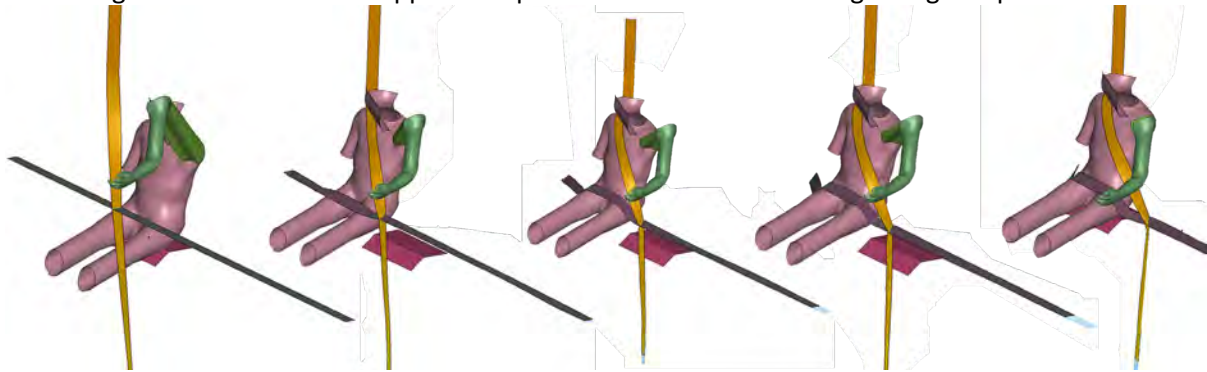


Fig. 13. Belt routing simulation at 0 ms, 25 ms, 50 ms, 75 ms, 100 ms (left to right).

Final Simulation

The settled positions and stress/strain states of the PIPER HBM, booster, and bench from the final settled position were used as starting positions for the final simulations. The post-processed seatbelt from the seatbelt routing simulation was included as well. An FMVSS 213 acceleration pulse [24] was applied to the model, starting at time 0 ms. This pulse had a ΔV of 48 km/hr and a peak acceleration of 24 g. The only other input applied to the model was a gravity 1 g acceleration vertically downwards to represent gravity. The final simulation was defined to have a run time of 120 ms, selected based on initial simulations to ensure that the simulations were run at least to the time of maximum forward head and pelvis excursion.

III. RESULTS

Simplified Booster Generation

Table II above provides the final list (and range) of parameters used to define the inputs for the automated booster generation and simulation pipeline (in addition to the posture and lap belt anchor location variables). After thorough stress testing and troubleshooting, the automatic booster generation process proved to be robust across the parameters (and parameter relationships) listed in Table II. Each booster was checked to ensure that the cushion did not extend past the end of the bench, and that it did not interfere with the bench cushion or bench seatback. Processes were developed to identify potential irregularities in the automation pipeline and to keep these booster seats from progressing to the final simulation. Potential issues included the booster seat shifting out from underneath the HBM during settling, seatbelt twisting during the routing simulation, and penetration between the seatbelt and HBM or wide lap belt guide. Testing indicated that 96% of booster seats successfully reached the final simulation and 93% of the booster seats successfully completed the final simulation.

Two comparisons were tested to examine the performance of the simplifications made in this process. The first was to compare the response of the booster included with the PIPER software to a simplified booster generated with the simplified geometric parameters matching that booster. The second was to compare the responses of a booster with the low-density foam material model, and a booster with a uniform pressure airbag material model, as shown in Fig. 14. These two comparisons exhibited similar results between the reference and simplified cases, with the only exception being that slightly more forward pelvis excursion was exhibited in the airbag booster compared to the booster modeled with low-density foam.

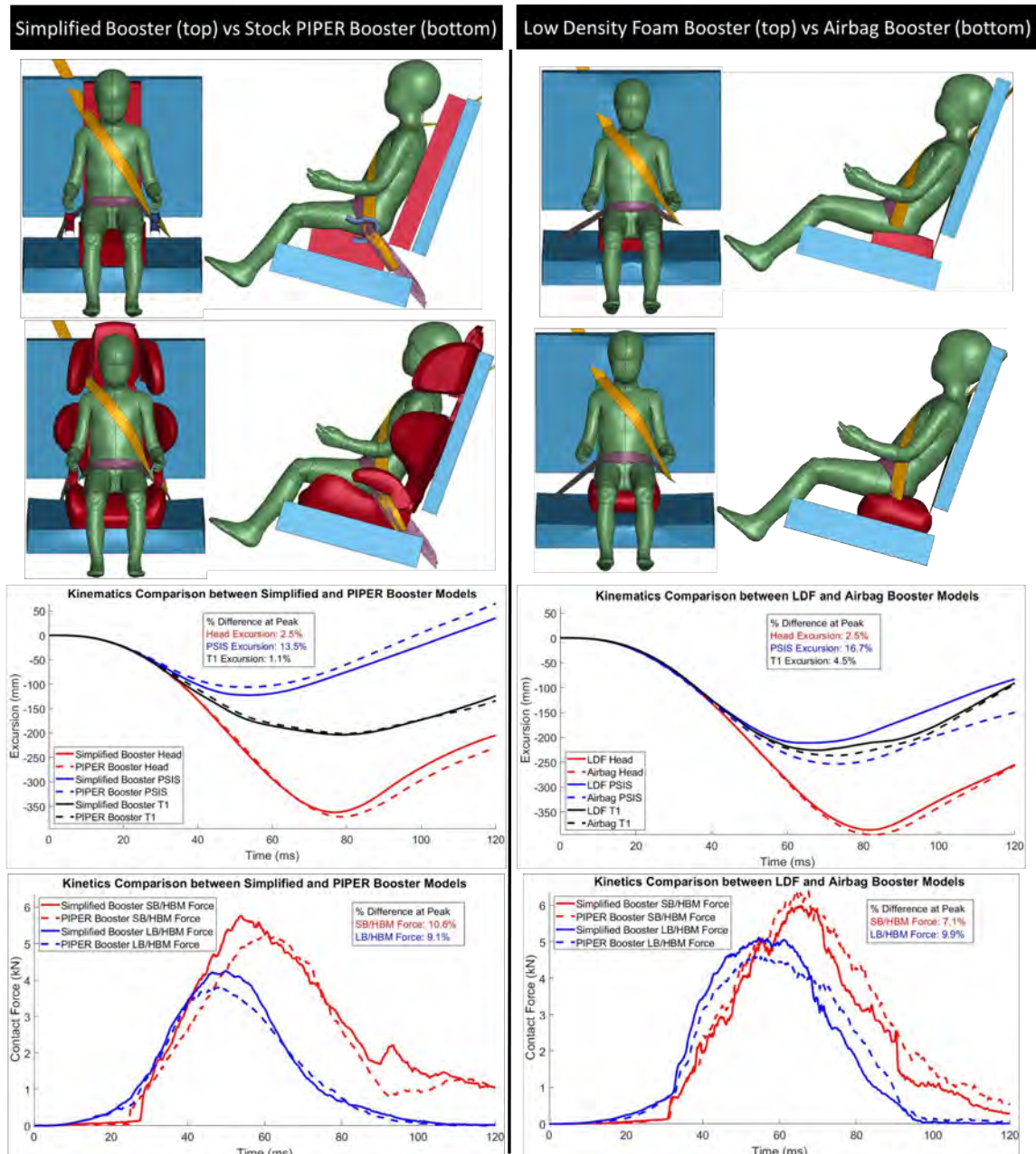


Fig. 14. Left: Geometric simplification test with Simplified PIPER booster (top) versus PIPER booster (bottom). Right: Low stiffness simplification test with Low density foam model (top) versus airbag model (bottom).

Automation Pipeline




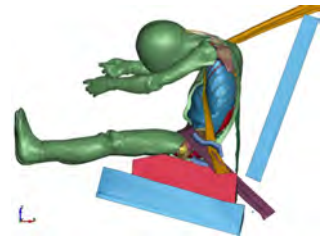

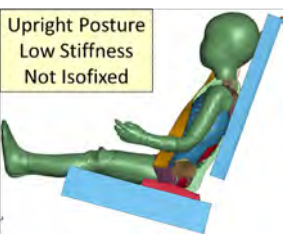

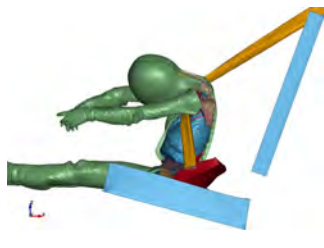







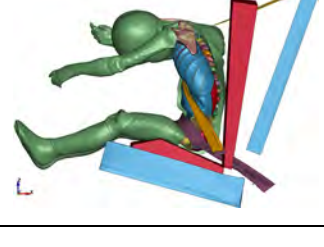



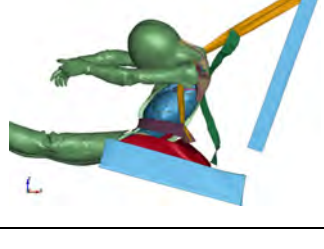

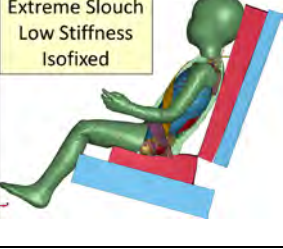

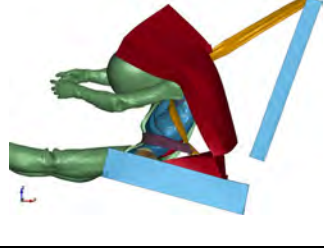
The automation pipeline resulted in a process that was orders of magnitude faster than the comparable manual approach. Table III details the average time required for each step. This represents computation time, as the steps did not require manual interaction. Steps 4, 5 and 6 utilized cluster computing to allow 30 boosters to be simulated in parallel using 20 CPUs per simulation for steps 4 and 6, and 12 CPUs for step 5. The finalized automation was capable of moving 30 boosters entirely through the pipeline in less than one day, with the bottleneck being the cluster capacity and not the model setup or pipeline automation itself.

TABLE III
AUTOMATION PIPELINE TIME REQUIRED

Step	Name	Average Time per Booster
1	Sampling	< 1 minute
2	Booster Model Generation	< 1 minute
3	HBM Positioning	< 1 minute
4	Settling Simulation	11 hours
5	Seatbelt Routing	14 minutes
6	Final Simulation	4 hours

Table IV shows the HBM response for six example boosters processed through the automation pipeline. These examples demonstrate the variability of initial position and seatbelt placement driven by booster geometry, booster stiffness, belt guides, and HBM posture. They include high and low stiffness boosters, constrained and unconstrained boosters, and upright through slouched occupant postures. The examples also illustrate the wide resulting range of occupant responses, with variation in head excursion, pelvis excursion and submarining. Example boosters #2, #5, and #6 all exhibited submarining. These three boosters also exhibited the largest head excursions, and made up three of the four largest pelvis excursions.

TABLE IV
EXAMPLE BOOSTERS

	Initial Position		Response at 80 ms	
Example Booster #1		Moderate Slouch High Stiffness Isofixed 		
Example Booster #2		Upright Posture Low Stiffness Not Isofixed 		
Example Booster #3		Moderate Slouch High Stiffness Not Isofixed 		
Example Booster #4		Upright Posture High Stiffness Not Isofixed 		
Example Booster #5		Extreme Slouch Low Stiffness Not Isofixed 		
Example Booster #6		Extreme Slouch Low Stiffness Isofixed 		

IV. DISCUSSION

The results indicate that this automation pipeline is an effective way of simulating large numbers of booster seats. While the design and implementation of the automation suite is a significant investment of time and resources, the end result is that the human interaction bottleneck is removed from the process. Using this method, study size is limited only by the available computational resources. Studies with hundreds, or thousands, of individual booster seats can utilize powerful data analysis techniques, such as meta-modeling and machine learning, gaining insights into the entire design space rather than just the individually tested data points. The process presented here was initially stress-tested with a test batch of 30 sampled booster designs. Since the conclusion of this initial development, the process has simulated more than 700 automatically generated boosters spanning the design space observed in the field (with analysis underway, to report in future studies).

Reducing the description of a booster seat to 20 parameters results in a simplified booster without many of the structures commonly seen on booster seats, such as side wings and contoured arm rests. Initial validation tests indicate that the simplified booster performs in a comparable manner to complex boosters that have more detailed structures (Fig. 14). The current validation testing is limited to frontal impacts. The booster parameterization process was designed with a focus on frontal impacts and significant modifications, to include side structures, would likely be necessary if it were applied to alternative crash modes.

Initial validation simulations also indicate that the low-density foam and airbag material models perform in a functionally similar manner. This simplification was necessary for successful implementation into the automation processes, as it was not feasible to integrate airbag inflation into the settling simulations across all possible booster geometries. Minor variations in the response are expected due to the differences in the Lagrangian low density foam formulation and the Eulerian uniform pressure airbag formulation. The variation observed in pelvis excursion may be due in part to the additional shearing ability of the airbag booster relative to the low-density foam booster, allowing for further pelvis motion. These differences are expected, and the purpose of this work was not to perfectly mimic the performance of airbag boosters but rather to examine the general effect of booster stiffness across a range representative of that expected to occur across current designs. In effect, these results indicate that the current representation with the low-density foam results in a conservative estimate of the effect of low stiffness, as the model with an airbag-style implementation tends to result in more forward motion of the pelvis. To verify these observations, we plan to further evaluate geometry-specific results with matched airbag and foam-type models outside of the automation pipeline in follow-on simulations.

Utilizing three different HBM postures allows for the evaluation of the robustness of booster seat performance when used with non-ideal postures. Out-of-position postures are common with children using booster seats, and the degree of slouch of the child may be related to the geometry of the booster seat and the vehicle seat [20]. As a result, it would be pertinent to evaluate the performance robustness of booster seats not only with an upright occupant but also with postures representing the range of those likely to occur with that booster geometry.

This work expands on the simulation automation processes presented in previous studies [12] and introduces additional functionality and complexity. Integrating parametrically generated booster seats into the automation pipeline increases the overall complexity of the process, as the HBM must be located in an individualized position for each booster, and the seatbelt routing algorithm must be capable of dealing with the varied booster configurations and geometries. This represents one of the most complex simulation automation problems present in automobile safety research. In the past, model positioning, settling and belt routing have relied on manual processes that create a bottleneck reliant on human intervention and time. As such, most parametric studies with HBMs have been constrained to studying a single geometry (anthropometry, posture, belt fit), varying only those characteristics that do not affect the initial model geometry [25–27]. The few studies that have sought to include geometry in parametric modeling have been limited in simulation sample size (e.g. 100 simulations or less), noting constraints placed by “semi-automated” processes [28]. Fully automated simulation processes equipped to include differences in geometry provide a means to evaluate not only differences in restraint geometry but also the robustness of safety systems accounting for potential differences in occupant anthropometry and posture [12]. The ability to evaluate safety system robustness in the face of diversity and variability is the major strength of simulation-based approaches, but has long proved elusive for human body modeling. These results demonstrate simulation automation for varied geometries and postures is possible and that it is feasible for even the most challenging simulation setup problems in automobile safety today.

V. CONCLUSIONS

This study sought to develop an automated simulation methodology to generate and simulate parametrically-defined booster seats spanning the range of the current booster seat design space. Booster-related factors included the geometry and stiffness of the booster cushion and seatback, the location and type of booster belt guides, and constraint via ISOFIX (vs. unconstrained). In addition, the simulation pipeline was designed to evaluate the robustness of the booster performance across two different lap belt anchor positions and three different occupant postures (upright, moderate slouch, extreme slouch). The automation process was stress-tested with 30 automatically generated models spanning different booster designs postures and belt geometries. The process proved robust, providing a range of booster models spanning the current design space, and a corresponding diversity in occupant responses (in terms of kinematics and submarining). This methodology provides a means to investigate the effects and interactions of booster design characteristics across the diverse multi-dimensional space present in current booster designs, and advances tools for large-scale parametric simulation to leverage human body modeling to evaluate safety system robustness.

VI. ACKNOWLEDGEMENTS

This study was supported by a grant from the Insurance Institute for Highway Safety. The opinions presented here are solely those of the authors, and do not necessarily represent the consensus views of the funding organization.

VII. REFERENCES

- [1] Centers for Disease Control and Prevention. Web-based Injury Statistics Query and Reporting System (WISQARS), 2019 Unintentional Fatal Injury Data. 2019.
- [2] Durbin DR, Hoffman BD, COUNCIL ON INJURY, VIOLENCE, AND POISON PREVENTION. Child Passenger Safety. *Pediatrics*, 2018, 142(5):e20182460.
- [3] Arbogast KB, Jermakian JS, Kallan MJ, Durbin DR. Effectiveness of Belt Positioning Booster Seats: An Updated Assessment. *PEDIATRICS*, 2009, 124(5):1281–1286.
- [4] Jermakian J, Edwards M. Kinematics Comparison between the Hybrid III 6 Year-old with Standard Pelvis and Modified Pelvis with Gel Abdomen in Booster Sled Tests. 2017, :14.
- [5] Visvikis C, Thurn C, Müller T. Investigation of Different Methods of Improving the Assessment of Booster Seats in Light of Dummy and Sensor Capabilities. 2020, :12.
- [6] Durbin DR, Elliott MR, Winston FK. Belt-Positioning Booster Seats and Reduction in Risk of Injury Among Children in Vehicle Crashes | *Pediatrics* | JAMA | JAMA Network. no date.
- [7] Durbin DR, Arbogast KB, Moll EK. Seat belt syndrome in children: A case report and review of the literature: *Pediatric Emergency Care*, 2001, 17(6):474–477.
- [8] Hoy GA, Cole WG. The paediatric cervical seat belt syndrome. *Injury*, 1993, 24(5):297–299.
- [9] Arbogast KB, Kent RW, et al. Mechanisms of Abdominal Organ Injury in Seat Belt-Restrained Children. *Journal of Trauma: Injury, Infection & Critical Care*, 2007, 62(6):1473–1480.
- [10] Byard R, Noblett H. Child booster seats and lethal seat belt injury. *Journal of Paediatrics and Child Health*, 2004, 40(11):639–641.
- [11] Gepner B, Draper D, et al. Comparison of Human Body Models in Frontal Crashes with Reclined Seatback. *IRCOBI 2019 Conference*, 2019.
- [12] Perez-Rapela D, Forman JL, Huddleston SH, Crandall JR. Methodology for vehicle safety development and assessment accounting for occupant response variability to human and non-human factors. *Computer Methods in Biomechanics and Biomedical Engineering*, 2020, :1–16.

- [13] Bohman K, Östh J, et al. Booster cushion design effects on child occupant kinematics and loading assessed using the PIPER 6-year-old HBM and the Q10 ATD in frontal impacts. *Traffic Injury Prevention*, 2020, :1–6.
- [14] Berntsson J. A Parametric Study of Shoulder Belt Interactions with the PIPER Scalable Child Human Body Model in Frontal and Frontal Offset Impacts. no date, :111.
- [15] Maheshwari J, Duong N, Sarfare S, Belwadi A. Evaluating the response of the PIPER scalable human body model across child restraining seats in simulated frontal crashes. *Traffic Injury Prevention*, 2018, 19(sup2):S140–S142.
- [16] Forman J, Michaelson J, Kent R, Kuppa S, Bostrom O. Occupant Restraint in the Rear Seat: ATD Responses to Standard and Pre-tensioning, Force-Limiting Belt Restraints. *Annals of Advances in Automotive Medicine (AAAM)*, 2008, 52:13.
- [17] Jolliffe IT. *Principal Component Analysis*, Springer-Verlag, New York, 2002.
- [18] Kirkpatrick S, Gelatt CD, Vecchi MP. Optimization by Simulated Annealing. *Science*, 1983, 220(4598):671–680.
- [19] *Booster Seat Belt Fit Evaluation Protocol Version IV*. 2018.
- [20] Jones MLH, Ebert S, Manary MA, Reed MP, Klinich KD. Child Posture and Belt Fit in a Range of Booster Configurations. *International Journal of Environmental Research and Public Health*, 2020, 17(3).
- [21] Gil Obando LM, López López A, Ávila CL. Normal values of the maximal respiratory pressures in healthy people older than 20 years old in the City of Manizales - Colombia. *Colombia Médica : CM*, no date, 43(2):119–125.
- [22] Beillas P, GIORDANO C, et al. Development and performance of the PIPER scalable child human body models, 14th International Conference on the Protection of Children in Cars, 2016, MUNICH, Germany.
- [23] Miller M, Perez-Rapela D, Gepner B, Jermakian J, Forman J. Examination of Restraint Sensitivity and Validation of the PIPER 6-Year-Old Model. *18th International Conference -- Protection of Children in Cars*, 2020, :6.
- [24] *LABORATORY TEST PROCEDURE for FMVSS 213 Child Restraint Systems*. 2014.
- [25] Joodaki H, Gepner B, Kerrigan J. Leveraging machine learning for predicting human body model response in restraint design simulations. *Computer Methods in Biomechanics and Biomedical Engineering*, 2020, 0(0):1–15.
- [26] Hu J, Wu J, et al. Optimizing the Rear Seat Environment for Older Children, Adults, and Infants. *Traffic Injury Prevention*, 2013, 14(sup1):S13–S22.
- [27] Hu J, Reed MP, et al. Optimizing Seat Belt and Airbag Designs for Rear Seat Occupant Protection in Frontal Crashes, 2017.
- [28] Hu J, Zhang K, et al. Frontal crash simulations using parametric human models representing a diverse population. *Traffic Injury Prevention*, 2019, 20(sup1):S97–S105.
- [29] *Federal Motor Vehicle Safety Standards; Child Restraint Systems, Incorporation by Reference*. 2020.
- [30] *Wietholter K, Loudon A, Burton R. Evaluation of Seat Foams for the FMVSS No. 213 Test Bench*. 2016.
- [31] *Manary MA, Klinich KD, Orton N, Eby B, Weir Q. Development of a Surrogate Shoulder Belt Retractor for Sled Testing Of Booster Seats*. 2019.

APPENDICES

APPENDIX A

Booster Test Sample

TABLE A1
BOOSTER CHARACTERIZATION SAMPLE

Mfg	Model	Type	Latch	Material	Mass (kg)	LB Guide	SB Guide
Cosco	Finale 2-in-1	Highback	Yes	Plastic	3.62	Wide	Fixed
MaxiCosi	Rodifix	Highback	Yes	Plastic	6.36	Wide	Fixed
Graco	TurboBooster	Combination	Yes	Plastic	4.03	Wide	Fixed/Flexible
Eddie Bauer	Deluxe Highback 65	Highback	No	Plastic	5.44	Wide	Fixed
Diono	Monterey XT	Combination	Yes	Plastic	6.48	Wide	Fixed/Flexible
Graco	TurboBooster TakeAlong	Combination	Yes	Plastic	4.505	Wide	Fixed/Flexible
Graco	Nautilus Snuglock	Combination	Yes	Plastic	5.68	Wide	Fixed/Flexible
Safety 1st	Summit 65	Highback	Yes	Plastic	5.24	Wide	Fixed
Harmony	Elite 3-in-1 Defender 360	Combination	Yes	Plastic	7.64	Wide	Fixed/Flexible
Evenflo	Big Kid	Combination	No	Plastic	2.86	Wide	Fixed/Flexible
Urbini	Asenti	Highback	Yes	Plastic	7.95	Wide	Fixed
Harmony	Folding Travel Booster	Highback	No	Plastic	3.87	Wide	Fixed
Kids Embrace	Fun-Ride Spiderman	Combination	No	Plastic	4.19	Wide	Fixed/Flexible
Britax	Highpoint	Highback	Yes	Plastic	5.32	Wide	Fixed
Evenflo	Spectrum	Combination	No	Plastic	5.29	Wide	Fixed/Flexible
Diono	Radian 3R	Highback	Yes	Plastic	10.52	Narrow	Fixed
Aidia	Explorer 2-in-1	Combination	No	Plastic	3.85	Wide	Fixed/Flexible
Graco	Argos 80	Combination	Yes	Plastic	9.39	Narrow	Fixed/Flexible
Cosco	Highback 2-in-1	Highback	Yes	Plastic	3.42	Wide	Fixed
Chicco	KidFit	Combination	Yes	Plastic	4.63	Wide	Fixed
Diono	Cambria	Combination	Yes	Plastic	5.38	Wide	Fixed
Cybox	Solution M-Fix	Highback	No	Plastic	6.48	Wide	Fixed
Evenflo	EveryStage	Highback	Yes	Plastic	9.89	Wide	Fixed
Peg-Perego	Viaggio Shuttle Plus 120	Combination	Yes	Plastic	6.84	Wide	Fixed
Jane	Montecarlo R1	Highback	No	Plastic	6.81	Wide	Fixed
Safety 1st	Elite EX 100 Air +	Highback	No	Plastic	10.73	Wide	Fixed
little tikes	Highback Booster Seat	Highback	No	Plastic	3.82	Wide	Fixed
Kiddy	Cruiser 3	Highback	Yes	Plastic	7.33	Wide	Fixed
Chicco	MyFit	Highback	Yes	Plastic	10.76	Wide	Fixed
Nuna	aace	Combination	No	Plastic	7.15	Wide	Fixed
Harmony	Big Boost Deluxe	Backless	Yes	Plastic	1.53	Wide	Flexible
LilFan	No Back Booster Seat	Backless	No	Plastic	1.01	Wide	Flexible
Chicco	GoFit	Backless	No	Plastic	2.24	Wide	Flexible
Safety 1st	Incognito	Backless	No	Foam	0.25	Flexible Slipping	Free
Diono	Rainier	Highback	No	Plastic	11.32	Narrow	Fixed
Graco	Nautilus Snuglock	Combination	Yes	Plastic	9.56	Wide	Fixed/Flexible
RideSafer	Delighter	Backless	No	Plastic	0.78	Wide	None
Aidia	Scout	Backless	No	Plastic	1	Wide	Flexible
little tikes	Booster Seat	Backless	No	Plastic	1.09	Wide	Flexible
mifold	Grab-and-Go Booster	Backless	No	Plastic	0.69	Fixed Slipping	Flexible
hiccapop	uberboost	Backless	No	Air	0.51	Flexible Slipping	Flexible
Eddie Bauer	Storage Booster	Backless	No	Plastic	2.32	Wide	Flexible
BubbleBum	Booster	Backless	No	Air	0.45	Flexible Slipping	Flexible
Evenflo	Chase	Highback	No	Plastic	3.65	Wide	Rigid

APPENDIX B
Sampling Dependencies

This appendix provides additional detail as to how observed correlations within the booster test sample were implemented into the sampling algorithm.

Seatback Depth at Bight

Backless booster seats were assigned a value of zero for the seatback depth at bight. The value was sampled independently for full boosters.

Cushion Depth at Bight

Sampling for the cushion depth at bight parameter was defined differently for full and backless boosters to account for the fact that the observed ranges were different between the two booster styles (Fig. A1).

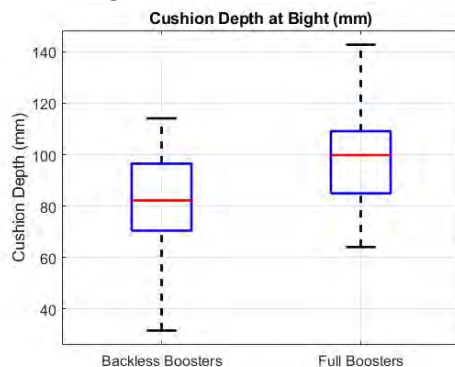


Fig. A1. Cushion Depth at Bight comparison between backless and full boosters

For backless boosters, cushion depth at bight was sampled independently based on the values recorded for backless boosters in the test sample. For full boosters, cushion depth at bight was sampled dependently with noise based on the observed relationship with seatback depth at bight. Fig. A2 below shows the values from the test sample in blue, the fit linear relationship model in red, and the 95% confidence interval for value prediction in pink. The value for cushion depth at bight could be sampled anywhere between the two confidence interval lines.

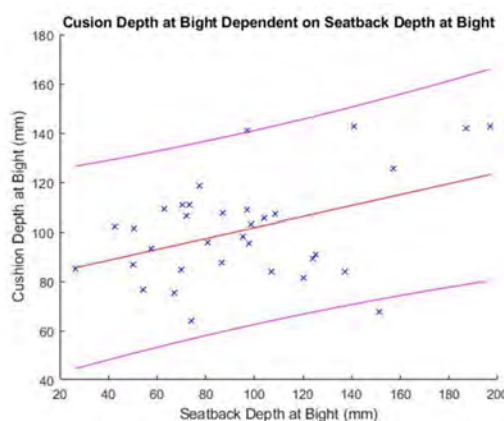


Fig. A2. Observed relationship between Seatback Depth at Bight and Cushion Depth at Bight. Blue crosses are test sample data points, the red line shows the fit linear relationship, and the pink lines show bounding 95% confidence intervals.

Lap Belt Guide Position and Angle

Lap belt guide position and angle were sampled independently, but the available ranges for these values were adjusted based on the type of lap belt guide. Each lap belt guide type was sampled only within the areas observed in the test sample. The wide c lap belt guide position window was further broken down into three distinct regions, each of which had a different maximum and minimum angle. This accounted for the fact that wide c lap belt guides located in the aft region tended to have a more vertical angle, while wide c lap belt guides located in the low, forward area tended to have more horizontal angles Fig. A3 shows the locations of the lap belt guides from the test sample, as well as the position windows and minimum/maximum angles in

each region. The slipping window does not have an angle range defined, as the slipping lap belt guides were not assigned an angle.

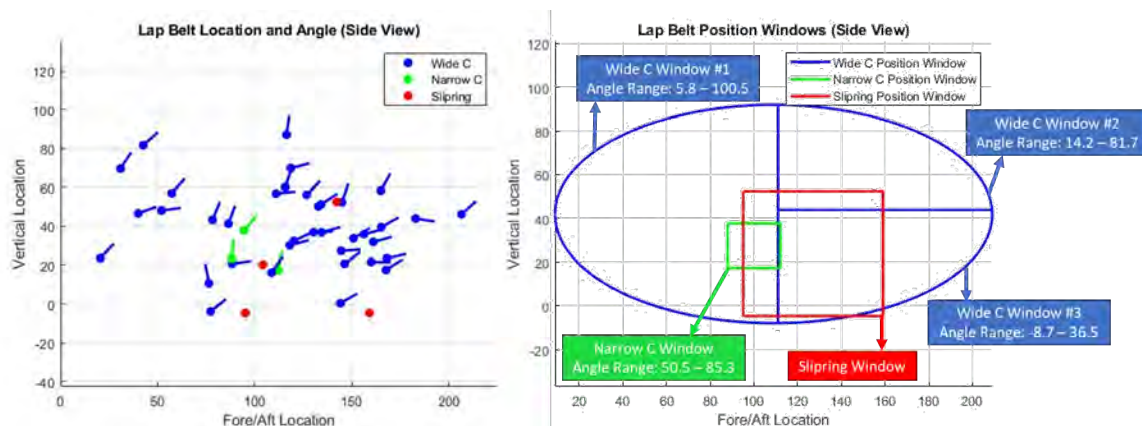


Fig. A3. Observed lap belt guide locations (left) and sampling windows (right)

Shoulder Belt Guide Position

The position of the shoulder belt guide was not applicable to backless boosters, as the backless boosters were equipped with either a flexible shoulder belt guide placed directly over the shoulder or no shoulder belt guide at all. For full boosters, the position of the shoulder belt guide was sampled only within the window observed in the test sample. Fig. A4 shows the locations of the shoulder belt guides from the test sample, as well as the shoulder belt guide position window used in the sampling.

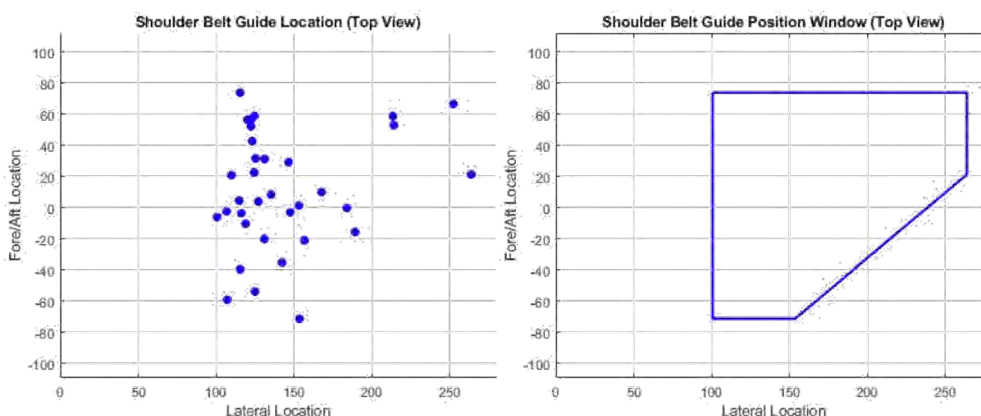


Fig. A4. Observed shoulder belt guide locations (left) and sampling window (right).

Seatback Depth at 300 mm

The seatback depth at 300 mm was a secondary parameter in this analysis. Therefore, it was defined directly from its relationship with seatback depth at bight rather than sampled with additional noise. Fig. A5 shows the relationship between the two parameters. All seatback depth at 300 mm values were generated along the line of best fit from the relationship with seatback depth at bight.

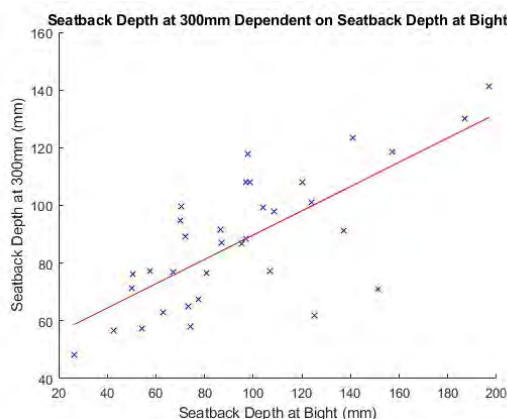


Fig. A5. Observed relationship between Seatback Depth at Bight and Seatback Depth at 300 mm.

Cushion Segment Lengths

Cushion Segment 1 Length was a secondary parameter in this analysis. Therefore, it was defined directly from its relationship with Total Cushion Length rather than sampled with additional noise. Fig. A6 shows the relationship between Total Cushion Length and Cushion Segment 1 Length. All Cushion Segment 1 Length values were generated along the line of best fit based on the booster’s Total Cushion Length value. Cushion Segment 2 Length was a secondary parameter in this analysis. Cushion Segment 2 Length was defined directly by subtracting Cushion Segment 1 Length from Total Cushion Length.

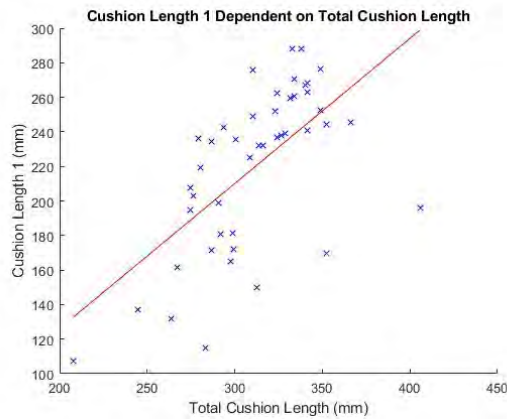


Fig. A6: Observed relationship between Total Cushion Length and Cushion Segment 1 Length.

Cushion Segment 2 Angle

Cushion Segment 2 Angle was a secondary parameter in this analysis. Therefore, it was defined directly from its relationship with Cushion Segment 1 Angle rather than sampled with additional noise. Fig. A7 shows the relationship between Cushion Segment 1 Angle and Cushion Segment 2 Angle. All Cushion Segment 2 Angle values were generated along the line of best fit based on the booster’s Cushion Segment 1 Angle value.

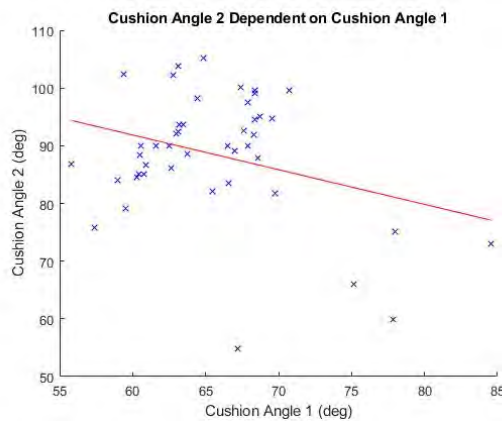


Fig. A7. Observed relationship between Cushion Segment 1 Angle and Cushion Segment 2 Angle.

APPENDIX C
Updated FMVSS 213 Bench Finite Element Model Development

The FMVSS 213 bench was selected as a representative rear seat for this study, as it is the industry standard for child restraint testing. An FE model of the bench was developed, including the proposed improvements to the FMVSS 213 bench [29]. Some of these changes include geometry modifications, seat foam updates, and the addition of a retractor. Seat geometry was determined using technical drawings of the updated bench seat. The seat was simplified by approximating all steel and aluminium seat structures as rigid and omitting them from the model (Fig. A8). This resulted in only the two cushion pieces remaining, with the rear of the bench seatback and the bottom of the bench cushion rigidly fixed in the model.

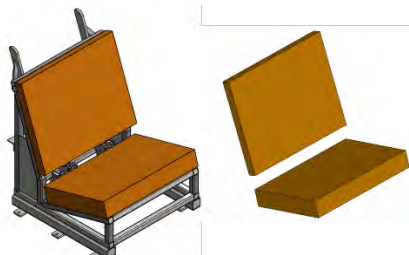


Fig. A8. Comparison of FMVSS 213 CAD model (left) and simplified FE model (right).

The material used in the original FMVSS 213 bench model was less stiff than the real-world rear-seat models tested by NHTSA. The new proposed seat foam material, called the NHTSA-Woodbridge material, is more representative of the rear-seat stiffness of the fleet [30]. This material was modeled in LS-DYNA using the Low Density Foam material card, which was selected due to its previous use in FE models, its ability to exhibit damping and hysteresis, and its stability in high compression/high energy environments. The properties of this material were tuned to match dynamic impact test data published by NHTSA [30]. The results of this tuning showed that the FE foam material was able to capture the hysteresis seen in the real-world test bench (Fig. A9). The seatbelt retractor model was selected based on NHTSA’s development of a surrogate shoulder belt retractor for booster seat sled testing [31]. The retractor model provides a force of 14 N for the first 50.8 mm of belt payout, after which it locks and does not pay out any more belt. A coordinate system was defined for the bench, with the origin at the centreline of the seat bight. With directions relative to a seated occupant, the X, Y, and Z axes extended aft, right, and up, respectively. This was defined as the global coordinate system for all simulations.

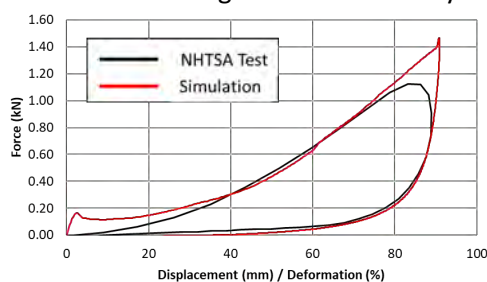


Fig. A9. Force vs displacement of foam and foam model.

The completed FE booster seat model was tested in comparison with a sled test of the Graco Turbo Booster on the FMVSS 213 bench. This test was selected as a point of comparison as the Graco booster was the most similar to the PIPER booster of the available sets of test data (Fig. A10). This is not a perfect comparison, as there are geometric differences between the real-world Graco Booster and the FE PIPER booster, as well as differences between the ATD and the PIPER model.

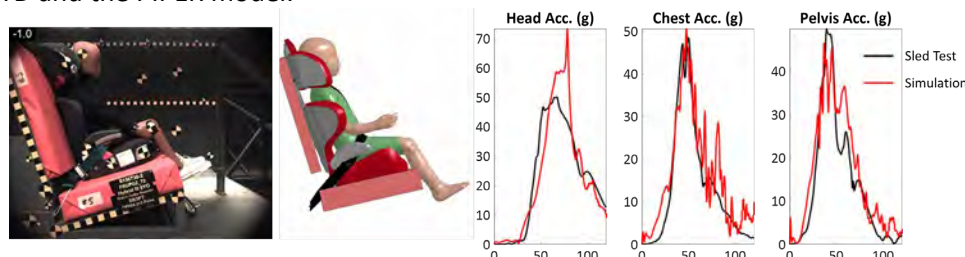


Fig. A10. Graco Turbo Booster sled test (left) versus PIPER booster FE test (middle), and results (right).

APPENDIX D

HBM Positioning Algorithm

The following algorithm was used to position each HBM as closely as possible to the final settled position without interfering with the booster or bench. An example of the step-wise process is shown in Fig. 12.

TABLE A2
HBM POSITIONING ALGORITHM

Step	Algorithm Process
1	Translate model such that the pelvis is the appropriate distance from the seatback based on the sampled posture value
2a	Select PIPER model with the most extreme back angle that does not interfere with the seatback
2b	If the least extreme back angle still interferes with the seatback, rotate the model by 1 degree increments until there is no longer interference
3a	Check distance between PIPER model and booster cushion segment 1
3b	If the PIPER model interferes with the cushion segment 1, translate PIPER upwards along the seatback coordinate system in order to maintain appropriate distance between pelvis and seatback
3c	If the PIPER model is above cushion segment 1, translate downward along seatback coordinate system until 2 mm above cushion segment 1
4	Repeat steps 3a, 3b and 3c for cushion segment 2
5a	Select PIPER model with least leg extension that does not interfere with the booster or bench cushion
5b	If the most extended leg model still interferes with the booster or bench cushion, translate PIPER upward along seatback coordinate system until there is no longer interference

APPENDIX E

Settling Constraints

Several constraints were added to the PIPER model to ensure that a realistic position was maintained throughout the settling simulations. These constraints are detailed in Table A3. The third entry in the table is of note, as that constraint maintained the HBM’s posture to the sampled value. Note that these constraints were not included in the final simulation run. Fig. A11 compares the settling results with and without the femur beam element.

TABLE A3
SETTLING CONSTRAINT DETAILS

Region	Type	Description
Arms	Constrained Rigid Bodies	The hand bones, radius and ulna of each arm were merged to the T4 vertebrae such that they could not rotate or translate independent of the vertebrae
Pelvis	Boundary SPC	The left and right PSIS nodes were not permitted to translate in the Y direction of the seatback coordinate system (medially/laterally), keeping the pelvis centered on the booster
Pelvis	Boundary SPC	The left and right PSIS nodes were not permitted to translate in the Z direction of the seatback coordinate system (fore/aft), keeping the distance between the pelvis and seatback consistent
Head	Constrained Extra Nodes	The nodes of the head coordinate system were merged to the T4 vertebrae such that the head could not rotate or translate independent of the vertebrae
Femurs	Beam Element	A beam element attached the two medial femoral condyles, keeping the legs from moving laterally on narrow low stiffness boosters
T1	Material Definition	The material definition of T1 was modified such that it was not permitted to translate in the global Y direction (medially/laterally)

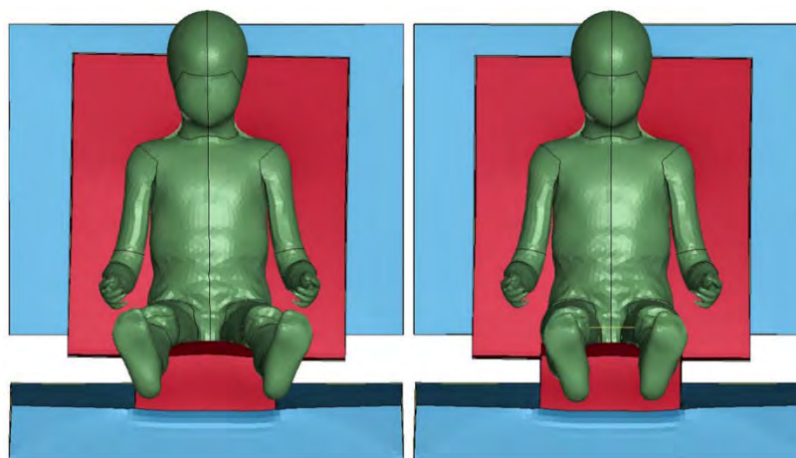


Fig. A11. Final settled position without (left) and with (right) femur beam constraint.

APPENDIX F

Seatbelt Routing Simulation Detail

The settled positions of the PIPER model and the booster were used as inputs for the seatbelt routing simulations. PIPER’s torso, thighs, left arm, and right side of the head and neck were rigidized and used in the simulation. This rigidized shell was further modified by extruding the end of the thighs and centreline of the face to encourage proper belt position. The top surface of the booster cushion was rigidized and used in the simulation as well (Fig. A12).

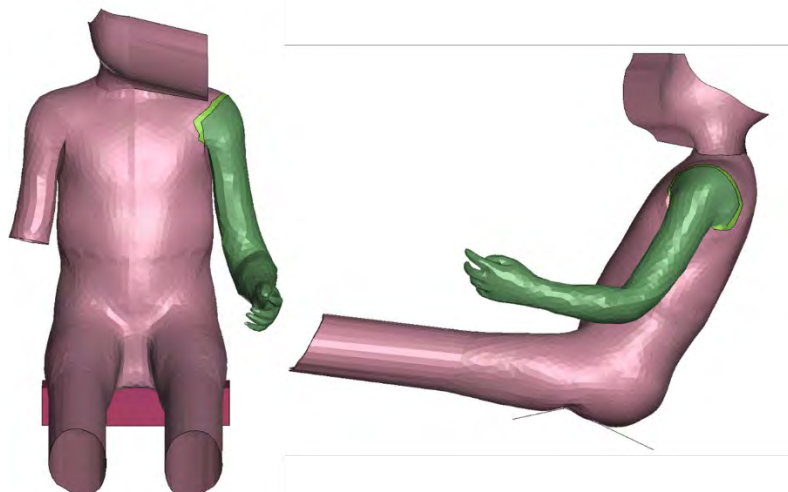


Fig. A12. Rigidized PIPER and booster shells used in seatbelt routing simulations.

The seatbelt routing prepositioning consisted of translating PIPER’s left arm upwards from its initial position and translating the remaining portions of PIPER and the booster seat surface down and away from their initial positions. The seatbelt was then imported in its stock position. During the simulation, PIPER and the booster seat surface were moved back to their original positions as the belts were being tightened. Moving the model into the belts as they tightened allowed the belts to find natural positions along the torso and thighs. The seatbelt routing simulations occur over a 100 ms time frame, with various part motions happening over that span. The step-by-step process for the seatbelt routing simulations is detailed in Table A4 and Fig. 13.

TABLE A4
SEATBELT ROUTING PROCESS

Step	Stage [Time]	Description
1	Pre-simulation	Extract positions of PIPER’s torso, thighs, left arm, and right side of face and neck from settling simulation
2	Pre-simulation	Extrude the ends of PIPER’s thighs and centreline of face
3	Pre-simulation	Translate PIPER’s left arm 100 mm left and 100 mm upward
4	Pre-simulation	Translate remaining portions of PIPER and booster seat surface 220 mm aft and 300 mm down
5	Pre-simulation	Import shoulder belt and lap belt in stock positions
6	Simulation [0–100 ms]	Translate seatbelt anchors to final positions, tightening belts
7	Simulation [0–30 ms]	Translate PIPER’s torso and thighs back to initial positions
8	Simulation [90–100 ms]	Translate PIPER’s left arm and booster surface back to initial position
9	Post-simulation	Post-process belt to prepare for final simulation

The seatbelt guides generated for each seatbelt routing simulation were dependent on the parameters generated by the sampling. There were three possible options for shoulder belt guide (free, flexible, and fixed), as well as four options for lap belt guide (wide, narrow, flexible, and fixed). Fig. 5 and Fig. 6 show real-world examples of these guide types. Each of these guides was modeled as slings in LS-DYNA with two exceptions. Boosters with a free shoulder belt guide did not attempt to guide the upper part of the shoulder belt, so no

slipping was used. Boosters with a wide lap belt guide utilized a separate part to guide the belt rather than a slipping. This allowed the belts freedom to move within the lap belt guide. The wide part shape was generated based on the wide profile shown in Fig. A13. Tables A5 and A6 provide additional detail about each guide type and the cases in which it was used, as different sampled belt guide setups required different arrangements. Fig. A14 shows an example of each guide type.

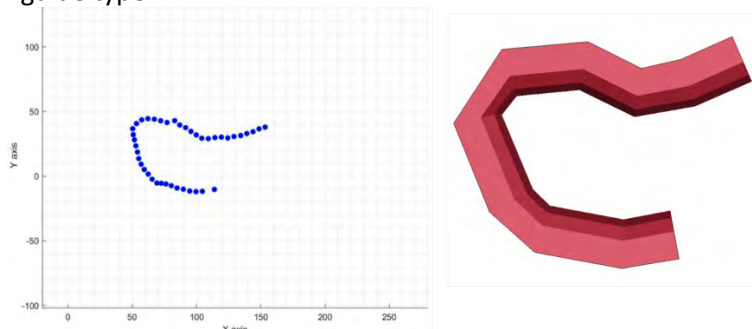


Fig. A13. Representative wide profile (left), wide profile part (right).

TABLE A5
SEATBELT GUIDE DESCRIPTIONS

Guide	Description
SR1	Upper shoulder belt slipping
SR2	Lower shoulder belt slipping
SR3	Seatbelt buckle
SR4	Right lap belt slipping
SR5	Left lap belt slipping
WC1	Right lap belt
WC2	Left lap belt

TABLE A6
SEATBELT GUIDE USE MATRIX

	Free Shoulder Belt Guide	Flexible Shoulder Belt Guide	Fixed Shoulder Belt Guide
Wide Lap Belt Guide	SR3, WC1, WC2	SR1, SR3, WC1, WC2	SR1, SR3, WC1, WC2
Narrow Lap Belt Guide	SR2, SR3, SR4, SR5	SR1, SR2, SR3, SR4, SR5	SR1, SR2, SR3, SR4, SR5
Flexible Lap Belt Guide	SR3, SR4, SR5	SR1, SR3, SR4, SR5	SR1, SR3, SR4, SR5
Fixed Lap Belt Guide	SR3, SR4, SR5	SR1, SR3, SR4, SR5	SR1, SR3, SR4, SR5

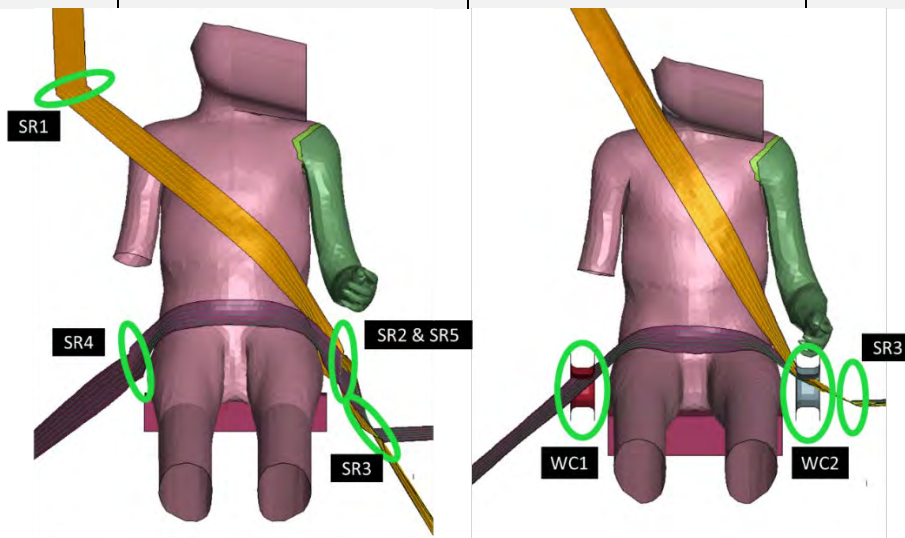


Fig. A14. Left: fixed shoulder belt guide, narrow lap belt guides. Right: free shoulder belt guide, wide lap belt guides.

Once the belt routing simulation was completed, the final positions of the belts were extracted and post-processed. This post-processing was comprised of trimming the excess length off the belts, as well as smoothing the mesh. Mesh smoothing was critical, as the short distance between the buckle slipping and belt guide slippings could result in a skewed mesh after simulation completion (Fig. A15).

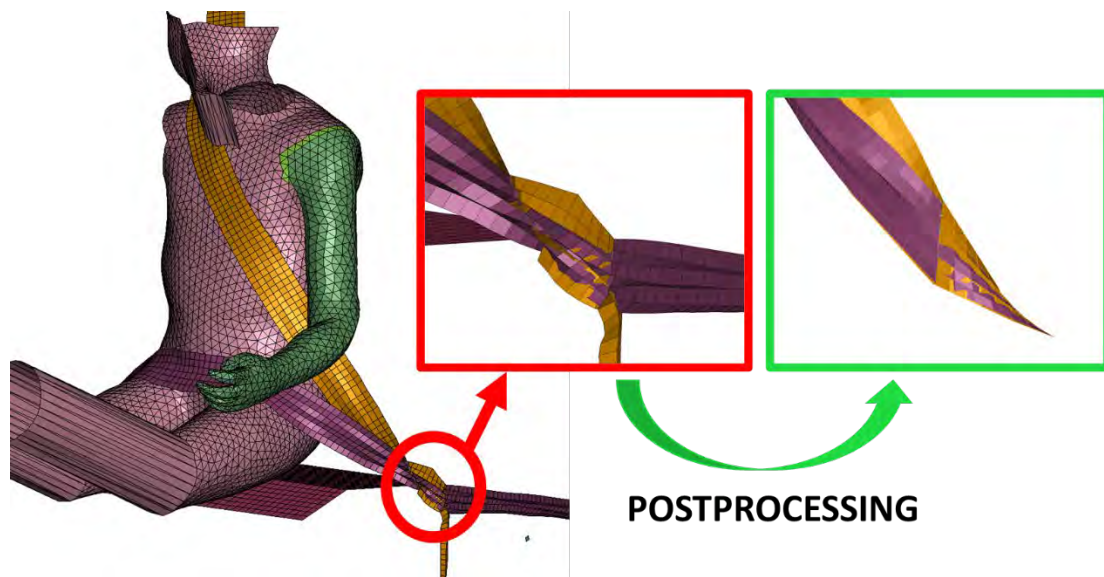


Fig. A15. Mesh smoothing post-processing.

Seatbelt post-processing applied to the seat belt guides as well, based on the belt guide types determined in the sampling process. The lap belt guide angle was defined relative to the first segment of the booster seat cushion for wide and narrow lap belt guides. The angles of the wide, narrow and fixed lap belt guides were not permitted to change during the final simulations, while the flexible lap belt guides were attached to a piece of fabric that permitted some rotation. Free, flexible and fixed were the available options for shoulder belt guides. Full boosters all utilized the fixed shoulder belt guide, while backless boosters could use either a flexible shoulder belt guide or no shoulder belt guide at all. Seatbelt guide attachment methods are detailed in Table A7.

TABLE A7
BELT GUIDE ATTACHMENT METHODS

	High Stiffness Booster	Low Stiffness Booster
Wide LBG	Part rigidly fixed to rigid bottom surface of booster cushion	Part rigidly fixed to a set of 12 nodes on aft bottom surface of booster cushion
Narrow LBG	Slipping rigidly fixed to rigid bottom surface of booster cushion	Slipping rigidly fixed to a set of 12 nodes on aft bottom surface of booster cushion
Flexible LBG	Slipping fixed to one end of 20 mm piece of fabric, other end rigidly fixed to rigid bottom surface of booster cushion	Slipping fixed to one end of 20 mm piece of fabric, other end rigidly fixed to 10 closest nodes on side surface of booster cushion
Fixed LBG	Slipping rigidly fixed to rigid bottom surface of booster cushion	Slipping rigidly fixed to 10 closest nodes on side surface of booster cushion
Free SBG	N/A (no slipping used)	N/A (no slipping used)
Flexible SBG	Slipping connected to one end of flexible leash, other end rigidly fixed to rigid bottom surface of booster cushion	Slipping connected to one end of flexible leash, other end connected to a set of 12 nodes on aft bottom surface of booster cushion
Fixed SBG	Slipping rigidly fixed to rigid aft surface of booster seatback	Slipping rigidly fixed to 10 closest nodes of aft surface of booster seatback